# Analysis of the Finite Element Approximability of Three-Dimensional Time-Harmonic Electromagnetic Problems Involving Bianisotropic Materials and Metamaterials

Praveen Kalarickel Ramakrishnan* Mario Rene Clemente Vargas†
Mirco Raffetto‡

May 5, 2020

## 1 Introduction

## 2 Mathematical description of the problem

In this paper we are interested in electromagnetic problems that involves bianisotropic media under time-harmonic excitation, which was studied in [1]. While the full details of the problem definition and results are available in the reference, here we provide a summary of main points in order to ease the understanding of the present developments.

The problem is formulated in a domain $\Omega \in \mathbb{R}^3$ which has a boundary denoted by $\Gamma$. The time harmonic sources imply that all the resulting fields are in turn time-harmonic and the assumed factor $e^{j\omega t}$ is ubiquitous and is suppressed. The media involved in the problem is linear and time-invariant and is considered to satisfy the following constitutive relations:

$$\begin{cases} \mathbf{D} = (1/c_0)\, P\, \mathbf{E} + L\, \mathbf{B} & \text{in } \Omega, \\ \mathbf{H} = M\, \mathbf{E} + c_0\, Q\, \mathbf{B} & \text{in } \Omega. \end{cases} \tag{1}$$

In the above equation, $\mathbf{E}$, $\mathbf{B}$, $\mathbf{D}$ and $\mathbf{H}$ are complex valued functions defined in $\Omega$ and represent, respectively, the electric field, magnetic induction, electric displacement, magnetic field and $c_0$ is the speed of light in vacuum. The space where we will seek $\mathbf{E}$ and $\mathbf{H}$ is [2] (p. 82; see also p. 69)

$$U = H_{L^2,\Gamma}(\mathrm{curl}, \Omega) = \{\mathbf{v} \in H(\mathrm{curl}, \Omega) \mid \mathbf{v} \times \mathbf{n} \in L_t^2(\Gamma)\}, \tag{2}$$

where [2] (p. 48)

$$L_t^2(\Gamma) = \{\mathbf{v} \in (L^2(\Gamma))^3 \mid \mathbf{v} \cdot \mathbf{n} = 0 \ \text{ almost everywhere on } \Gamma\}. \tag{3}$$

*Department of Electrical, Electtronic, Telecommunications Engineering and Naval Architecture, University of Genoa, Via Opera Pia 11a, I-16145, Genoa, Italy, email:pravin.nitc@gmail.com
†Department of Electrical, Electtronic, Telecommunications Engineering and Naval Architecture, University of Genoa, Via Opera Pia 11a, I-16145, Genoa, Italy, email:mario.clemente@unige.it
‡Department of Electrical, Electtronic, Telecommunications Engineering and Naval Architecture, University of Genoa, Via Opera Pia 11a, I-16145, Genoa, Italy, email:raffetto@dibe.unige.it

Based on Maxwell's equations, boundary conditions and constitutive relations, the following variational formulation of the problem can be deduced [3]: given $\omega > 0$, electric and magnetic current densities $\mathbf{J}_e, \mathbf{J}_m \in (L^2(\Omega))^3$ and the known term $\mathbf{f}_R \in L_t^2(\Gamma)$, involved in admittance boundary condition, find $\mathbf{E} \in U$ such that

$$a(\mathbf{E}, \mathbf{v}) = l(\mathbf{v}) \quad \forall \mathbf{v} \in U, \tag{4}$$

where

$$\begin{aligned} a(\mathbf{u}, \mathbf{v}) = c_0\big(Q \operatorname{curl} \mathbf{u}, \operatorname{curl} \mathbf{v}\big)_{0,\Omega} - \frac{\omega^2}{c_0}\big(P\,\mathbf{u}, \mathbf{v}\big)_{0,\Omega} - j\omega\big(M\,\mathbf{u}, \operatorname{curl} \mathbf{v}\big)_{0,\Omega} \\ -j\omega\big(L \operatorname{curl} \mathbf{u}, \mathbf{v}\big)_{0,\Omega} + j\omega\big(Y\,(\mathbf{n} \times \mathbf{u} \times \mathbf{n}), \mathbf{n} \times \mathbf{v} \times \mathbf{n}\big)_{0,\Gamma} \end{aligned} \tag{5}$$

and

$$l(\mathbf{v}) = -j\omega\big(\mathbf{J}_e, \mathbf{v}\big)_{0,\Omega} - c_0\big(Q\,\mathbf{J}_m, \operatorname{curl} \mathbf{v}\big)_{0,\Omega} + j\omega\big(L\,\mathbf{J}_m, \mathbf{v}\big)_{0,\Omega} - j\omega\big(\mathbf{f}_R, \mathbf{n} \times \mathbf{v} \times \mathbf{n}\big)_{0,\Gamma}. \tag{6}$$

In [1] we derived certain sufficient conditions that guarantee the well posedness and finite element approximability of the problem. The developed theory was applied to problems involving rotating axisymmetric objects. In this paper we apply the theory to a wider range of problems involving bianisotropic media, demonstrating the generality of the developments and obtaining interesting new solutions. In particular we show how the theory can be applied in the presence of metamaterials by considering the equivalent media of the type discussed in literature [4], [5], [6].

It could be also useful to recall some points on how to check for the sufficient conditions that ensure the well posedness and finite element approximability of the problem. In particular it was observed that most of the hypotheses are easily verified for important practical problems. It turns out that the most critical conditions that need to be verified are conditions (9) and (10) in [1]. These conditions are restated in the following equations.

$$\text{for every } \mathbf{v} \in U, \mathbf{v} \neq 0, \quad \sup_{\mathbf{u} \in U} |a(\mathbf{u}, \mathbf{v})| > 0, \tag{7}$$

$$\text{we can find } \alpha : \inf_{\mathbf{u} \in U,\ \|\mathbf{u}\|_U = 1} \sup_{\mathbf{v} \in U,\ \|\mathbf{v}\|_U \leq 1} |a(\mathbf{u}, \mathbf{v})| \geq \alpha > 0. \tag{8}$$

As described in [1], to satisfy the above conditions, we need to verify HM9-HM15 in the paper. Before stating these critical hypotheses a few definitions need to be made. $\Omega$ is decomposed into $m$ subdomains $\Omega_i$, $i \in I = \{1, 2, ...m\}$. This decomposition can be made such that $I = I_a \cup I_b$, where $I_a$ is characterized by subdomains where $L = M = 0$. Also, an alternative form of constitutive relations given in (9) is made use of to state some of the hypotheses [7].

$$\begin{cases} \mathbf{E} = \kappa\,\mathbf{D} + \chi\,\mathbf{B} & \text{in } \Omega, \\ \mathbf{H} = \gamma\,\mathbf{D} + \nu\,\mathbf{B} & \text{in } \Omega. \end{cases} \tag{9}$$

The local continuity of the tensors $P$, $Q$, $L$ and $M$ can be assumed in most practical problems and which allows the definiton of the following constants.

- $\exists C_L > 0$: $|(L \operatorname{curl} \mathbf{u}, \mathbf{v})_{0,\Omega}| \leq C_L \|\operatorname{curl} \mathbf{u}\|_{0,\Omega} \|\mathbf{v}\|_{0,\Omega}$ for all $\mathbf{u} \in H(\operatorname{curl}, \Omega)$ and $\mathbf{v} \in (L^2(\Omega))^3$,
- $\exists C_M > 0$: $|(M\,\mathbf{u}, \operatorname{curl} \mathbf{v})_{0,\Omega}| \leq C_M \|\mathbf{u}\|_{0,\Omega} \|\operatorname{curl} \mathbf{v}\|_{0,\Omega}$ for all $\mathbf{u} \in (L^2(\Omega))^3$ and $\mathbf{v} \in H(\operatorname{curl}, \Omega)$.

Now the important hypotheses are restated here and are renamed as H1-H7.

**H1.** $\exists\exists C_{\kappa,d} > 0,\, C_{\nu,d} > 0 : |determinant\,(\kappa)\,| \geq C_{\kappa,d},\, |determinant\,(\nu)\,| \geq C_{\nu,d},\, \forall \mathbf{x} \in \overline{\Omega}_i, \forall i \in I,$

**H2.** $\mathbf{l}_{1,3}^T\,\kappa^{-1}\,\mathbf{l}_{1,3} \neq 0,\ \mathbf{l}_{1,3}^T\,\nu^{-1}\,\mathbf{l}_{1,3} \neq 0\ \forall \mathbf{l}_{1,3} \in \mathbb{R}^3, \mathbf{l}_{1,3} \neq 0,\ \forall \mathbf{x} \in \overline{\Omega}_i,\ \forall i \in I_a,$

**H3.** $\exists\exists C_{\kappa,r} > 0,\ C_{\nu,r} > 0 :\ |\mathbf{l}_{1,3,n}^T\,\kappa^{-1}\,\mathbf{l}_{1,3,n}| \geq C_{\kappa,r},\ |\mathbf{l}_{1,3,n}^T\,\nu^{-1}\,\mathbf{l}_{1,3,n}| \geq C_{\nu,r}\ \forall \mathbf{l}_{1,3,n} \in \mathbb{R}^3 :\ \|\mathbf{l}_{1,3,n}\|_2 = 1,\ \forall \mathbf{x} \in \overline{\Omega}_i,\ \forall i \in I_b,$

**H4.** $\exists\exists C_{\kappa,s} > 0, C_{\nu,s} > 0$:

$$\big(\sum_{i,j=1}^{3} |\kappa_{ij}|\big) - \min_{i=1,2,3} |\kappa_{ii}| \leq C_{\kappa,s} \quad \forall \mathbf{x} \in \overline{\Omega}_k,\ \forall k \in I_b, \tag{10}$$

$$\big(\sum_{i,j=1}^{3} |\nu_{ij}|\big) - \min_{i=1,2,3} |\nu_{ii}| \leq C_{\nu,s} \quad \forall \mathbf{x} \in \overline{\Omega}_k,\ \forall k \in I_b, \tag{11}$$

and $\kappa$, $\chi$, $\gamma$ and $\nu$ satisfy

$$\frac{4\left(\big(\sum_{i,j=1}^{3} |\gamma_{ij}|\big) - \min_{i=1,2,3} |\gamma_{ii}|\right)\left(\big(\sum_{i,j=1}^{3} |\chi_{ij}|\big) - \min_{i=1,2,3} |\chi_{ii}|\right)}{\big(-C_{\kappa,s} + \sqrt{C_{\kappa,s}^2 + 4\,C_{\kappa,d}\,C_{\kappa,r}}\big)\,\big(-C_{\nu,s} + \sqrt{C_{\nu,s}^2 + 4\,C_{\nu,d}\,C_{\nu,r}}\big)} < 1 \tag{12}$$

$\forall \mathbf{x} \in \overline{\Omega}_k,\ \forall k \in I_b.$

**H5.** We can find $C_{PS} > 0$ such that $|(P\mathbf{u}, \mathbf{u})_{0,\Omega}| \geq C_{PS}\|\mathbf{u}\|_{0,\Omega}^2$ for all $\mathbf{u} \in (L^2(\Omega))^3$.

**H6.** We can find $C_{QS} > 0$ such that $|(Q\mathrm{curl}\,\mathbf{u}, \mathrm{curl}\,\mathbf{u})_{0,\Omega}| \geq C_{QS}\|\mathrm{curl}\,\mathbf{u}\|_{0,\Omega}^2$ for all $\mathbf{u} \in H(\mathrm{curl}, \Omega)$.

**H7.** $C_{PS}$, $C_{QS}$, $C_L$ and $C_M$ (i.e., all media involved) are such that $C_{QS} - \frac{C_L C_M}{C_{PS}} > 0$.

The section "some hints to apply the developed theory" of [1], provided the guidance to use the theory that was developed. Lemma 1 of the above paper provides a procedure to check conditions H5 and H6 and thus estimate the constants $C_{PS}$ and $C_{QS}$ which may in turn be used to check H7. Let $P$ be decomposed as $P = P_s - jP_{ss}$, and if $P_{ss}$ is uniformly positive definite in some region $\Omega_{el}$ and $P_s$ is uniformly positive definite in the complementary region $\Omega \setminus \Omega_{el}$, then H5 can be shown to be true in the following way. We can define $C_1 > 0$ and $C_2 > 0$ as follows.

$$\int_{\Omega_{el}} \mathbf{u}^* P_{ss}\mathbf{u} \geq C_1 \int_{\Omega el} |\mathbf{u}|^2 = C_1||\mathbf{u}||_{0,\Omega_{el}}^2\ \forall \mathbf{u} \in (L^2(\Omega))^3, \tag{13}$$

$$\left|\int_{\Omega\setminus\Omega_{el}} \mathbf{u}^* P_s\mathbf{u}\right| \geq C_2||\mathbf{u}||_{0,\Omega\setminus\Omega_{el}}^2. \tag{14}$$

The continuity of $P_s$ in $\Omega_{el}$ allows the definition of $C_3 > 0$ such that

$$\left|\int_{\Omega_{el}} \mathbf{u}^* P_s\mathbf{u}\right| \leq C_3\|\mathbf{u}\|_{0,\Omega_{el}}^2. \tag{15}$$

If $\Omega_{el} = \Omega$, then we can take $C_{PS} = C_1$, if $\Omega_{el} = \emptyset$ then $C_{PS} = C_2$ and in other cases

$$C_{PS} = \frac{1}{\sqrt{2}} \min\left(\sqrt{(1-\alpha)}C_2, \sqrt{C_1^2 + (1 - \frac{1}{\alpha})C_3^2}\right), \tag{16}$$

where $\alpha$ is such that $1 > \alpha > \frac{C_3^2}{C_1^2+C_3^2} > 0$.

Similar considerations can help to estimate $C_{QS}$ as well.

The values obtained above may not the best possible ones than can be estimated and the condition in H7 can be made less restrictive if the estimates of $C_{PS}$ and $C_{QS}$ can be higher. For example, whenever $P_s$ is uniformly definite in $\Omega$, we have $C_4 > 0$ such that

$$\left| \int_\Omega \mathbf{u}^* P_s \mathbf{u} \right| \geq C_4 ||\mathbf{u}||^2_{0,\Omega}. \tag{17}$$

In this case, the best value for $C_{PS}$ would be the larger among the one in (16) and $C_4$. Based on the definitions, the constants $C_L$ and $C_M$ can be estimated and the validity of H7 can be checked.

$$C_L = \max_{i \in I_b} \sup_{\mathbf{x} \in \Omega_i} \sqrt{\lambda_{max}(L^* L)} \tag{18}$$

and

$$C_M = \max_{i \in I_b} \sup_{\mathbf{x} \in \Omega_i} \sqrt{\lambda_{max}(M^* M)}, \tag{19}$$

As for the constants involved in H1-H4, the following considerations can be helpful.

$$C_{\kappa,d} = \min_{i \in I_b} \inf_{\mathbf{x} \in \Omega_i} |determinant(\kappa)|, \tag{20}$$

$$C_{\nu,d} = \min_{i \in I_b} \inf_{\mathbf{x} \in \Omega_i} |determinant(\nu)|, \tag{21}$$

$$C_{\kappa,s} = \max_{i \in I_b} \sup_{\mathbf{x} \in \Omega_i} \left( (\sum_{i,j=1}^{3} |\kappa_{ij}|) - \min_{i=1,2,3} |\kappa_{ii}| \right), \tag{22}$$

$$C_{\nu,s} = \max_{i \in I_b} \sup_{\mathbf{x} \in \Omega_i} \left( (\sum_{i,j=1}^{3} |\nu_{ij}|) - \min_{i=1,2,3} |\nu_{ii}| \right). \tag{23}$$

As for $C_{\kappa,r}$ and $C_{\nu,r}$ the following consideration might be helpful. By definition

$$C_{\kappa,r} = \min_{i \in I_b} \inf_{\mathbf{x} \in \Omega_i} \min_{\mathbf{l}_{1,3,n} \in \mathbb{R}^3 : \|\mathbf{l}_{1,3,n}\|_2 = 1} \sqrt{\left(\mathbf{l}_{1,3,n}^T \kappa_{is} \mathbf{l}_{1,3,n}\right)^2 + \left(\mathbf{l}_{1,3,n}^T \kappa_{iss} \mathbf{l}_{1,3,n}\right)^2}, \tag{24}$$

$$C_{\nu,r} = \min_{i \in I_b} \inf_{\mathbf{x} \in \Omega_i} \min_{\mathbf{l}_{1,3,n} \in \mathbb{R}^3 : \|\mathbf{l}_{1,3,n}\|_2 = 1} \sqrt{\left(\mathbf{l}_{1,3,n}^T \nu_{is} \mathbf{l}_{1,3,n}\right)^2 + \left(\mathbf{l}_{1,3,n}^T \nu_{iss} \mathbf{l}_{1,3,n}\right)^2}, \tag{25}$$

where $\kappa_{is}$ and $\kappa_{iss}$ are the symmetric matrices obtained by the usual decomposition of $\kappa^{-1}$ and similarly $\nu_{is}$ and $\nu_{iss}$ are those corresponding to $\nu^{-1}$. If both the symmetric matrices involved in the above expressions are semi-definite, then we can deduce the following lower bounds:

$$C_{\kappa,r} = \min_{i \in I_b} \inf_{\mathbf{x} \in \Omega_i} \sqrt{\left(\lambda_{min}(\kappa_{is})\right)^2 + \left(\lambda_{min}(\kappa_{iss})\right)^2}, \tag{26}$$

$$C_{\nu,r} = \min_{i \in I_b} \inf_{\mathbf{x} \in \Omega_i} \sqrt{\left(\lambda_{min}(\nu_{is})\right)^2 + \left(\lambda_{min}(\nu_{iss})\right)^2}. \tag{27}$$

If we also define

$$C_{\chi,s} = \max_{i \in I_b} \sup_{\mathbf{x} \in \Omega_i} \left( (\sum_{i,j=1}^{3} |\chi_{ij}|) - \min_{i=1,2,3} |\chi_{ii}| \right), \tag{28}$$

$$C_{\gamma,s} = \max_{i \in I_b} \sup_{\mathbf{x} \in \Omega_i} \left( (\sum_{i,j=1}^{3} |\gamma_{ij}|) - \min_{i=1,2,3} |\gamma_{ii}| \right), \tag{29}$$

the sufficient condition for the regularity used for proving uniqueness can be expressed as

$$K_u = \frac{4C_{\chi,s}C_{\gamma,s}}{\left(-C_{\kappa,s} + \sqrt{C_{\kappa,s}^2 + 4C_{\kappa,d}C_{\kappa,r}}\right)\left(-C_{\nu,s} + \sqrt{C_{\nu,s}^2 + 4C_{\nu,d}C_{\nu,r}}\right)} < 1. \tag{30}$$

# 3 Results and discussion

In this section we apply the theory developed in [1] to several different class to problems which could not be managed with the previous theory like the one in [3]. The conditions are established on the parameters of such problems, under which the well posedness and finite element approximability can be guaranteed. Under such condition, the numerical solutions for the fields are computed for the first time. The details of our finite element simulator is the same as that described in Section 5 of [1].

## 3.1 Plasmonic gratings considered in [4] behaving as bianisotropic metamaterial

In [4], the authors consider a plasmonic grating which exhibits bianisotropy at visible wavelength. Here we consider scattering problems involving an equivalent medium that can be characterized by the constitutive matrices of the same form given in the paper. The region occupied by the scatterer may be denoted as $\Omega_s \subset \Omega$. We start with the form of the normalized constitutive relation used in the paper [8], [9].

$$\epsilon = \varepsilon_0 \begin{bmatrix} \varepsilon_x & 0 & 0 \\ 0 & \varepsilon_y & 0 \\ 0 & 0 & \varepsilon_z \end{bmatrix}, \mu = \mu_0 \begin{bmatrix} \mu_x & 0 & 0 \\ 0 & \mu_y & 0 \\ 0 & 0 & \mu_z \end{bmatrix} \tag{31}$$

$$\xi = \frac{1}{c_0} \begin{bmatrix} 0 & 0 & 0 \\ 0 & 0 & 0 \\ 0 & j\xi_0 & 0 \end{bmatrix}, \zeta = \frac{1}{c_0} \begin{bmatrix} 0 & 0 & 0 \\ 0 & 0 & -j\xi_0 \\ 0 & 0 & 0 \end{bmatrix} \tag{32}$$

For the purposes of illustration we consider the homogeneous version of the equations in which $\varepsilon_x$, $\varepsilon_y$ and $\varepsilon_z$ are all set to a complex value $\varepsilon_r$. Moreover, $\mu_x$, $\mu_y$ and $\mu_z$ are each set equal to 1 and $\xi_0$ is real valued. This can be converted into the alternative form of constitutive relations [7] involving the $P$, $Q$, $L$, $M$ matrices defined in equation (1) and the final result is as shown the following equations.

$$P = c_0\varepsilon_0 \begin{bmatrix} \varepsilon_r & 0 & 0 \\ 0 & \varepsilon_r & 0 \\ 0 & 0 & \varepsilon_r - \xi_0^2 \end{bmatrix} \tag{33}$$

$$Q = \frac{1}{c_0\mu_0} I \tag{34}$$

$$L = M^T = \frac{j\xi_0}{\mu_0 c_0} \begin{bmatrix} 0 & 0 & 0 \\ 0 & 0 & 0 \\ 0 & 1 & 0 \end{bmatrix} \tag{35}$$

The complementary region $\Omega \setminus \Omega_s$ is occupied by the empty space, which, in our notation, is characterized by $P = c_0\varepsilon_0 I_3$, $Q = \frac{1}{c_0\mu_0} I_3$, $L = M = 0$.

The bianisotropic medium is lossy with the imaginary part $Im(\varepsilon_r) < 0$, where as $\xi_0$ is assumed real here to avoid some longer calculations. Now Lemma 1 of [1] can be applied to verify hypothesis H5. Inside $\Omega_s$, $P$ can be decomposed as $P = P_s - jP_{ss}$ with

$$P_s = \frac{P + P^*}{2} = c_0\varepsilon_0 \begin{bmatrix} Re(\varepsilon_r) & 0 & 0 \\ 0 & Re(\varepsilon_r) & 0 \\ 0 & 0 & Re(\varepsilon_r) - \xi_0^2 \end{bmatrix}, \tag{36}$$

and $P_{ss} = \frac{P^* - P}{2j} = -c_0\varepsilon_0 Im(\varepsilon_r) I_3$. Hence we have $\Omega_{el} = \Omega_s$, the lossy region where $P_{ss}$ is uniformly positive definite and the complementary region with free space where $P_s$ is uniformly positive definite. This means that the conditions of relevant Lemma are satisfied and as a result H5 is valid.

From the definitions $C_1 = c_0\varepsilon_0|Im(\varepsilon_r)|$, $C_2 = c_0\varepsilon_0$ and $C_3 = c_0\varepsilon_0 \max(|Re(\varepsilon_r) - \xi_0^2|, |Re(\varepsilon_r)|)$. To find the minimum of the two expressions in (16), we note that, in the valid range, the value of the first expression decreases monotonically with $\alpha$ where as that of the second expression increases with it. The highest estimate for $C_{PS}$ is obtained when the two expressions have the same value. The value of $\alpha$ at which this happens can be evaluated by equating the two expressions and finding the positive root of the resulting quadratic equation. This value of $\alpha$, denoted as $\alpha_{opt}$ is given by (37).

$$\alpha_{opt} = \frac{C_2^2 - C_1^2 - C_3^2 + \sqrt{(C_2^2 - C_1^2 - C_3^2)^2 + 4C_2^2C_3^2}}{2C_2^2} \tag{37}$$

Thus we may simply write

$$C_{PS} = \sqrt{\frac{1 - \alpha_{opt}}{2}} c_0\varepsilon_0. \tag{38}$$

As mentioned before, this does not mean that a better value of $C_{PS}$ cannot be found. For example, if $Re(\varepsilon_r) - \frac{\xi_0^2}{\mu_r} > 0$, then $P_s$ is uniformly positive definite in $\Omega$ and we can find another candidate for $C_{PS}$, namely $C_4 = c_0\varepsilon_0 \min(1, |Re(\varepsilon_r - )\xi_0^2|$. In particular, when $Re(\varepsilon_r) - \xi_0^2 > 1$, $C_4 = c_0\varepsilon_0$ is always going to give a value for $C_{PS}$ which is higher than that obtained from the Lemma.

The generality of out theory be clearly demonstrated by showing its applicability to bianisotropic metamaterials with non definite $P_s$ in $\Omega$. Hence in the rest of the subsection the discussion focuses on the cases with $\varepsilon_r < 0$. For this case,$C_3 = c_0\varepsilon_0|Re(\varepsilon_r) - \xi_0^2|$ , and we can directly use the value of $C_{PS}$ in (38). Since the material is assumed to be non magnetic the direct application of definition gives $C_{QS} = \frac{1}{c_0\mu_0}$ and H6 is valid. Likewise, the continuity constants $C_L = C_M = \frac{|\xi_0|}{c_0\mu_0}$. Then the inequality in H7 becomes $C_{QS} - \frac{C_L C_M}{C_{PS}} = \frac{1}{c_0\mu_0}(1 - \frac{\xi_0^2\sqrt{2}}{\sqrt{1-\alpha_{opt}}}) > 0$, which gives (39).

$$|\xi_0| < \left(\frac{1 - \alpha_{opt}}{2}\right)^{1/4}. \tag{39}$$

Since the right hand side of (39) also depends on $\xi_0$ due to the presence of $C_3$ in the expression for $\alpha_{opt}$, we do not have a closed form expression on the limit on $\xi_0$ below which H7 is satisfied. However a graphical analysis can be done for estimating such a limit on $|\xi_0|$, as shown in Figure 1. The value of $Re(\varepsilon_r)$ is varied in the range $(-1.0, -5.0)$ whereas $Im(\varepsilon_r)$ assumes values in the range $(-0.1, -0.5)$. It can be observed that for a fixed value of $Im(\varepsilon_r)$, the range of $\xi_0$ over

which H7 is valid steadily decreases as $|Re(\varepsilon_r)|$ increases. As for the dependence on $Im(\varepsilon_r)$, the corresponding range increases when medium becomes more lossy due to higher $|Im(\varepsilon_r)|$, as expected.

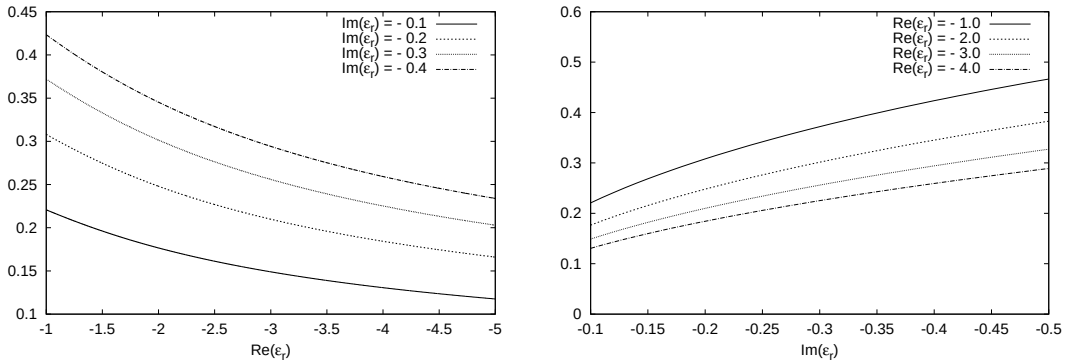


Figure 1: The magnitude of $|\xi_0|$ below which the condition 8 is satisfied as a function of $Re(\varepsilon_r)$ or $Im(\varepsilon_r)$ for media in [4]. The plot is for real $\xi_0$ negative values of $Re(\varepsilon_r)$ or $Im(\varepsilon_r)$ and the material is taken to be non magnetic.

We consider the alternative form of constitutive relations , which for the medium inside $\Omega_s$ becomes as in equations (40) to (42), for examining the validity of H1-H4 [7].

$$\kappa = \frac{1}{\varepsilon_0 \varepsilon_r} \begin{bmatrix} 1 & 0 & 0 \\ 0 & 1 & 0 \\ 0 & 0 & \frac{\varepsilon_r}{\varepsilon_r - \xi_0^2} \end{bmatrix} \tag{40}$$

$$\nu = \frac{1}{\mu_0} \begin{bmatrix} 1 & 0 & 0 \\ 0 & \frac{\varepsilon_r}{\varepsilon_r - \xi_0^2} & 0 \\ 0 & 0 & 1 \end{bmatrix} \tag{41}$$

$$\gamma = -\chi^T = \frac{j\xi_0 c_0}{\varepsilon_r - \xi_0^2} \begin{bmatrix} 0 & 0 & 0 \\ 0 & 0 & 1 \\ 0 & 0 & 0 \end{bmatrix} \tag{42}$$

Since H1-H4 needs to hold only locally, and they are trivially valid in the empty space outside the bianisotropic media, we have to just analyze them inside $\Omega_s$ occupied by the bianisotropic medium. These constants can be evaluated directly from the definitions. The determinants of $\kappa$ and $\nu$ are, respectively, $\frac{1}{(\varepsilon_0\varepsilon_r)^3(1-\frac{\xi_0^2}{\varepsilon_r})}$ and $\frac{1}{(\mu_0)^3(1-\frac{\xi_0^2}{\varepsilon_r})}$ which immediately give the values of $C_{\kappa,d}$ and $C_{\nu,d}$.

$$C_{\kappa,d} = \frac{1}{|\varepsilon_0^3 \varepsilon_r^3 (1 - \frac{\xi_0^2}{\varepsilon_r})|}, \tag{43}$$

$$C_{\nu,d} = \frac{1}{|\mu_0^3 (1 - \frac{\xi_0^2}{\varepsilon_r})|}. \tag{44}$$

The inverses of the diagonal matrices $\kappa$ and $\nu$ are just the diagonal matrices with the reciprocal entries. Applying equations (26) and (27) gives the values of $C_{\kappa,r}$ and $C_{\nu,r}$.

$$C_{\kappa,r} = |\varepsilon_0 \varepsilon_r (1 - \frac{\xi_0^2}{\varepsilon_r})|, \tag{45}$$

$$C_{\nu,r} = |\mu_0 (1 - \frac{\xi_0^2}{\varepsilon_r})|. \tag{46}$$

Using equations (22) and (23) we get the $C_{\kappa,s}$ and $C_{\nu,s}$.

$$C_{\kappa,s} = \frac{1}{\varepsilon_0} \max(\frac{2}{|\varepsilon_r|}, \frac{1}{|\varepsilon_r|}(1 + \frac{1}{|1 - \frac{\xi_0^2}{\varepsilon_r}|})), \tag{47}$$

$$C_{\nu,s} = \frac{1}{\mu_0} \max(2, (1 + \frac{1}{|1 - \frac{\xi_0^2}{\varepsilon_r}|})), \tag{48}$$

Since we are interested in the case when $Re(\varepsilon_r) < 0$ and real $\xi_0$, we see that $|1 - \frac{\xi_0^2}{\varepsilon_r}| > 1$, and the maximum reduces to the values in (49) and (50).

$$C_{\kappa,s} = \frac{2}{|\varepsilon_0 \varepsilon_r|}, \tag{49}$$

$$C_{\nu,s} = \frac{2}{\mu_0}. \tag{50}$$

From equations (29) and (28) we can easily evaluate $C_{\gamma,s}$ and $C_{\chi,s}$.

$$C_{\gamma,s} = C_{\chi,s} = |\frac{\xi_0 c_0}{\varepsilon_r - \xi_0^2}|. \tag{51}$$

The hypotheses H1-H3 are valid due to the existence of the above constants. Using these constants, the value of $K_u$ can be calculated from equation (30). The critical value of $|\xi_0|$ below which the condition in H4 is satisfied is plotted in Figure 2, with respect to either $Re(\varepsilon_r)$ or $Im(\varepsilon_r)$. The results show that the range of $\xi_0$ for which H4 holds true increases with the increase in $|Re(\varepsilon_r)|$, while it is practically independent of $Im(\varepsilon_r)$.

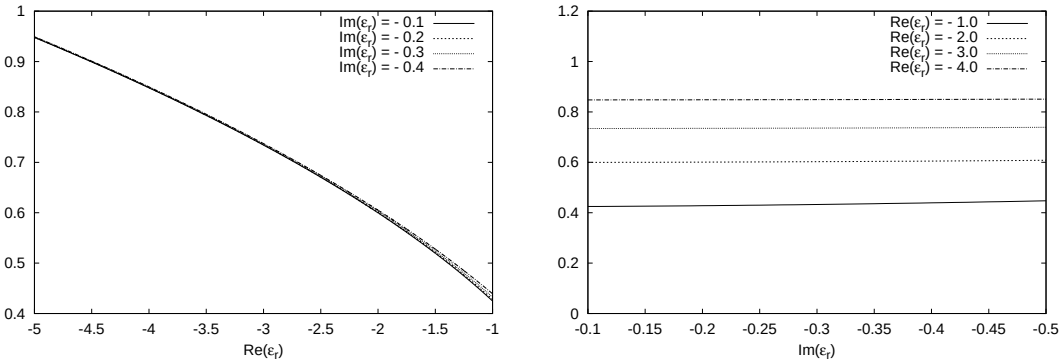


Figure 2: The magnitude of $\xi_0$ below which H4 is satisfied, as a function of $Re(\varepsilon_r)$ or $Im(\varepsilon_r)$ for media in [4]. The plot is for real $\xi_0$ and the material is taken to be non magnetic.

Let us try to understand the implications of the theory by applying it to the numerical solution of a specific problem involving the medium of interest. We consider the region with the

scatterer $\Omega_s$ to be a cube filled with homogeneous bianisotropic media. The surrounding region is filled with empty space and the overall domain of numerical investigation, $\Omega$, is of cubic shape as well, and is concentric to $\Omega_s$. In the following $\Omega$ is characterized by sides of length 2 $\mu m$ and $\Omega_s$ by those of 0.8 $\mu m$. The axes are taken along the sides of the cubes and the excitation is with a plane wave incident along the x axis, with electric field polarized along z axis, having a magnitude of 1 $V/m$ and wavelength of 1 $\mu m$.

Inside $\Omega_s$, the medium is characterized by $\varepsilon_r = -1 - j0.4$, $\mu_r = 1$ and $\xi_0 = -0.41$. This value is such that the hypotheses required for well posedness and finite element approximability are satisfied. In fact, for the $\varepsilon_r$ considered, condition 7 is valid for $|\xi_0| < 0.4235$ and condition 8 is valid for $|\xi_0| < 0.4393$.

The solutions are obtained with a first order edge element based Galerkin finite element method. The boundary condition is enforced with $Y$ equal to the admittance of vacuum and with an inhomogeneous term $\mathbf{f}_R$, taking into account the incident field.

The domain is discretized uniformly using tetrahedral meshes. The meshing is done by first dividing the domain into small identical cubes, each of which is in turn divided into six tetrahedra. The parameter $h$ denotes the maximum diameter of all the elements of the mesh [10] (p. 131), and in this case it is simply given by the side of the small cube times $\sqrt{3}$. To study the convergence of solution, we consider different levels of refinement of meshes ranked in order of $h$, ranging from "very coarse" to "very fine". For exmaple the mesh denoted very coarse is characterized by a cubes of sides 200 nm and the resulting mesh has 1331 nodes, 6000 tetrahedral elements and 1200 boundary faces. A summary of the information related to the four different refinements of the meshes that was used is given in Table 1.

| **Type of Mesh** | **Maximum Diameter of the Mesh ($h$ in nm)** | **Number of Nodes** | **Number of Elements** | **Number of Boundary Faces** |
|---|---|---|---|---|
| Very coarse | $200\sqrt{3}$ | 1331 | 6000 | 1200 |
| Coarse | $100\sqrt{3}$ | 9261 | 48000 | 4800 |
| Fine | $50\sqrt{3}$ | 68921 | 384000 | 19200 |
| Very fine | $25\sqrt{3}$ | 531441 | 3072000 | 76800 |

Table 1: Details of different meshes used.

The results related to the stability of the simulations are shown in Figure 3. The difference between sucessive refinements progressively decreases and the fine and very fine meshes give solution which are stable. The well posedness and convergnce result that was predicted using the theory guarantees that our solutions are reliable.

The magnitudes and pahses of some for the components of the field along different axis directions are shown in Figures 4 to 7. The solutions obtained for $\xi_0 = -0.41$ are compared with that for the isotropic case ($\xi_0 = 0$, $\varepsilon_r = -1 - j0.4$, $\mu_r = 1$). For example we can see in Figures 4 and 7 that there are differences of 10 to 20 percent of the incident field in the magnitudes of the electric fields which are induced by the magneto electric coupling factor $\xi_0$. Likewise the phases of the fields are similarly affected by the bianisotropy of the medium. These non negligible effects imply that the accuracy of the simulations requires the consideration of the bianisotropy of the medium. Hence the reliability of the finite element silution in the presence of bianisotropy is important for getting good results for this kind of problems. The appliaciton of our theory gives the conditions under which we can guarantee such reliability.

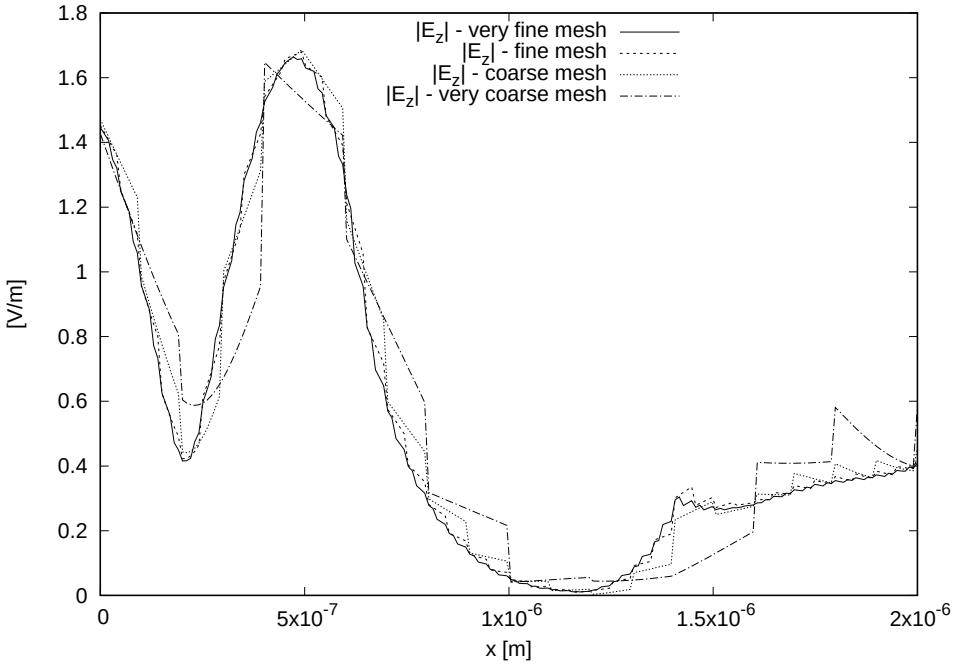


Figure 3: Convergence of the solution for problem involving medium in [4]. The magnitude of the $z$ component of the electric field is plotted along a line parallel to $x$ axis for four different meshes.

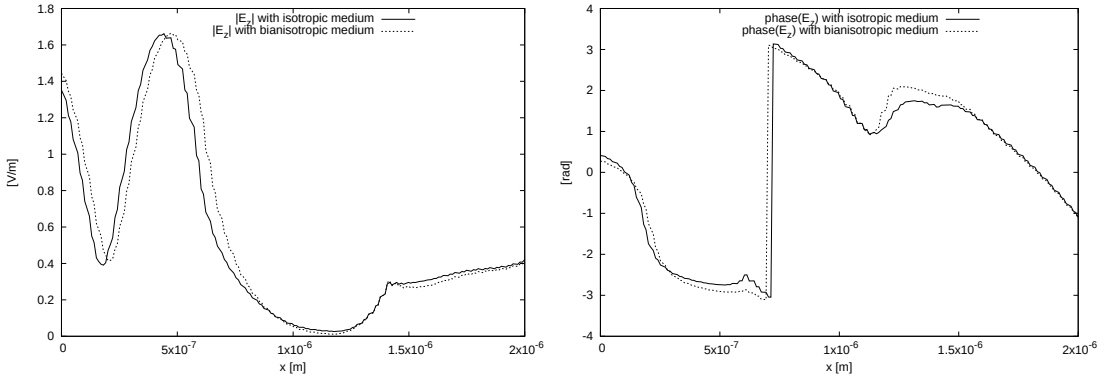


Figure 4: The magnitude and phase of the $z$ component of electric field along a line parallel to $x$ axis and passing though the center of gravity of the domain for problem involving medium in [4]. The plot for bianisotropic case using $\xi_0 = -0.41$ is compared with the solution obtained in isotropic case using $\xi_0 = 0$.

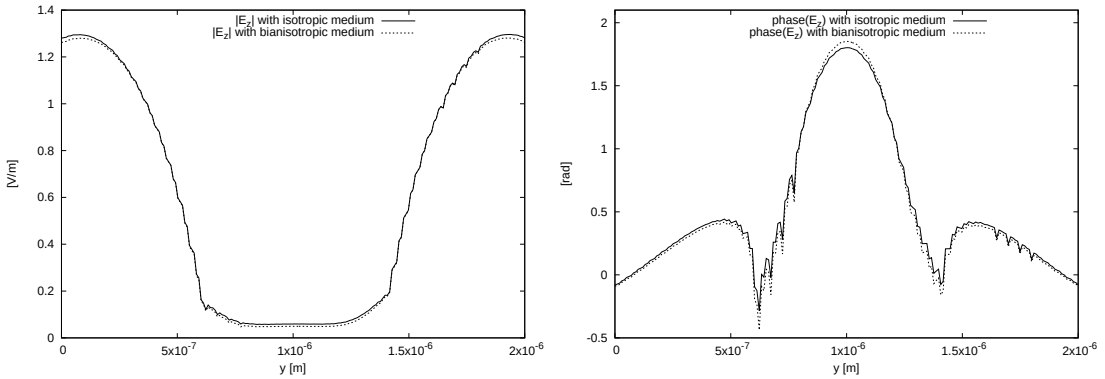


Figure 5: The magnitude and phase of the $z$ component of electric field along a line parallel to $y$ axis and passing though the center of gravity of the domain for problem involving medium in [4]. The plot for bianisotropic case using $\xi_0 = -0.41$ is compared with the solution obtained in isotropic case using $\xi_0 = 0$.

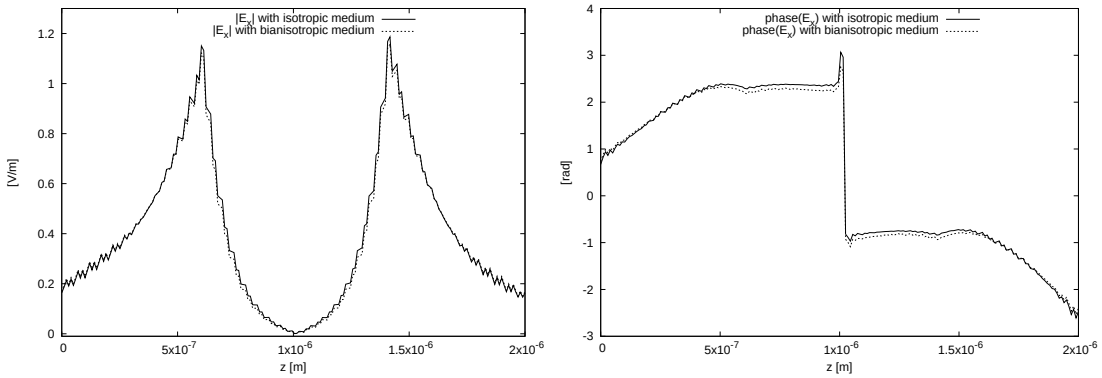


Figure 6: The magnitude and phase of the $x$ component of electric field along a line parallel to $z$ axis and passing though the center of gravity of the domain for problem involving medium in [4]. The plot for bianisotropic case using $\xi_0 = -0.41$ is compared with the solution obtained in isotropic case using $\xi_0 = 0$.

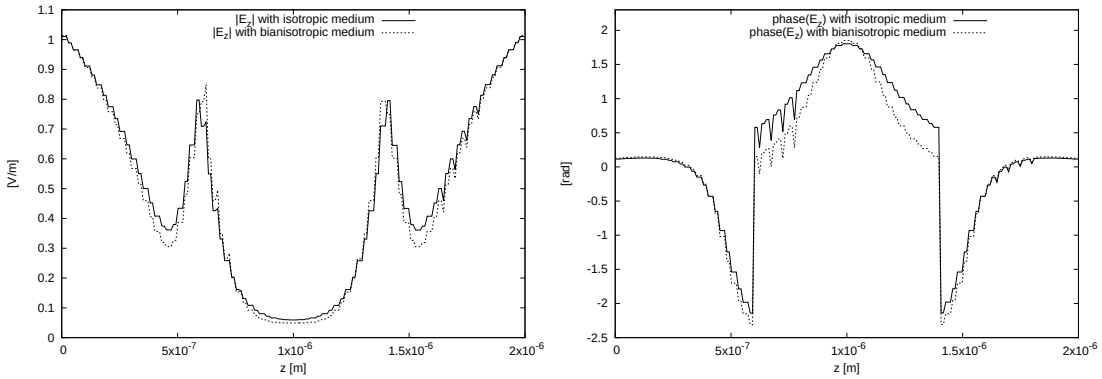


Figure 7: The magnitude and phase of the $z$ component of electric field along a line parallel to $z$ axis and passing though the center of gravity of the domain for problem involving medium in [4]. The plot for bianisotropic case using $\xi_0 = -0.41$ is compared with the solution obtained in isotropic case using $\xi_0 = 0$.

## 3.2 Chirowaveguides considered in [5]

In [5], the authors consider a metallic waveguide which is air filled except for an obstacle characterized by a chiral media with the following constitutive relations.

$$\begin{cases} \mathbf{D} = \varepsilon_0 \varepsilon_r I_3 \mathbf{E} - j\xi_c I_3 \mathbf{B} \\ \mathbf{H} = -j\xi_c I_3 \mathbf{E} + \frac{1}{\mu_0 \mu_r} I_3 \mathbf{B}. \end{cases} \tag{52}$$

Here $\varepsilon_r$, $\mu_r$ and $\xi_c$ are strictly positive real quantities. Thus from (1) we easily can easily identify $P$, $Q$, $L$ and $M$ which are given below.

$$P = \varepsilon_0 \varepsilon_r c_0 I_3 \tag{53}$$

$$Q = \frac{1}{\mu_0 \mu_r c_0} I_3 \tag{54}$$

$$L = M = -j\xi_c I_3 \tag{55}$$

In [3] it was shown that this media could not be managed by the previous theory developed there. However, the generality of the present theory allows us to apply it to obtain the conditions for well-posedness and finite element approximability of this kind of problem of practical interest.

Here we analyze the validity of the hypotheses by considering $\varepsilon_r > 1$ and $\mu_r = 1$. $P_s$ is equal to $\varepsilon_0 \varepsilon_r c_0$ inside material and simply $\varepsilon_0 c_0$ outside. Since $\Omega_{el} = \emptyset$, $C_{PS}$ is equal to $C_2$ defined in (14) and has a value $\varepsilon_0 c_0$, verifying the hypothesis H5. The hypothesis H6 is also trivially valid and $C_{QS} = \frac{1}{\mu_0 c_0}$. By equations (18) and (19), $C_L = C_M = |\xi_c|$. Then the inequality in hypothesis H7 becomes $C_{QS} - \frac{C_L C_M}{C_{PS}} = \frac{1}{c_0}(\frac{1}{\mu_0} - \frac{\xi_c^2}{\varepsilon_0}) > 0$ which implies

$$\xi_c < \sqrt{\frac{\varepsilon_0}{\mu_0}} = 2.654\,10^{-3} \text{ mho} . \tag{56}$$

This is not a small value considering the chiral effects reported in [5]. Now we need to verify the hypotheses H1-H4 which need to hold true locally and hence we have to examine only media inside the obstacle which is bianisotropic. For doing this the suitable form of constitutive relations is in terms of $\kappa$, $\nu$, $\gamma$ and $\chi$ which are given by the following [7].

$$\kappa = \frac{1}{\varepsilon_0 \varepsilon_r} I_3 \tag{57}$$

$$\nu = \frac{\varepsilon_0 \varepsilon_r + \mu_0 \xi_c^2}{\mu_0 \varepsilon_0 \varepsilon_r} I_3 \tag{58}$$

$$\chi = -\gamma = \frac{j\xi_c}{\varepsilon_0 \varepsilon_r} I_3 \tag{59}$$

$\kappa$ and $\nu$ are multiples of the identity matrix with eigenvalues $\varepsilon_0 \varepsilon_r$ and $(\frac{\varepsilon_0 \varepsilon_r + \mu_0 \xi_c^2}{\mu_0 \varepsilon_0 \varepsilon_r})$ respectively. The determinants are just the cubes of the eigenvalues and hence according to equations (20) and (21) we get the values of $C_{\kappa,d}$ and $C_{\nu,d}$

$$C_{\kappa,d} = \left(\frac{1}{\varepsilon_0 \varepsilon_r}\right)^3 \tag{60}$$

$$C_{\nu,d} = \left(\frac{\varepsilon_0 \varepsilon_r + \mu_0 \xi_c^2}{\mu_0 \varepsilon_0 \varepsilon_r}\right)^3 \tag{61}$$

$C_{\kappa,s}$ and $C_{\nu,s}$ by equations (22) and (23) are in this case simply twice the eigenvalue of corresponding diagonal matrix.

$$C_{\kappa,s} = \frac{2}{\varepsilon_0 \varepsilon_r} \tag{62}$$

$$C_{\nu,s} = 2\frac{\varepsilon_0 \varepsilon_r + \mu_0 \xi_c^2}{\mu_0 \varepsilon_0 \varepsilon_r} \tag{63}$$

The inverse of the matrices are also trivial and equations (26) and (27) simply evaluate to the reciprocals of eigenvalues of $\kappa$ and $\nu$ respectively giving $C_{\kappa,r}$ and $C_{\nu,r}$.

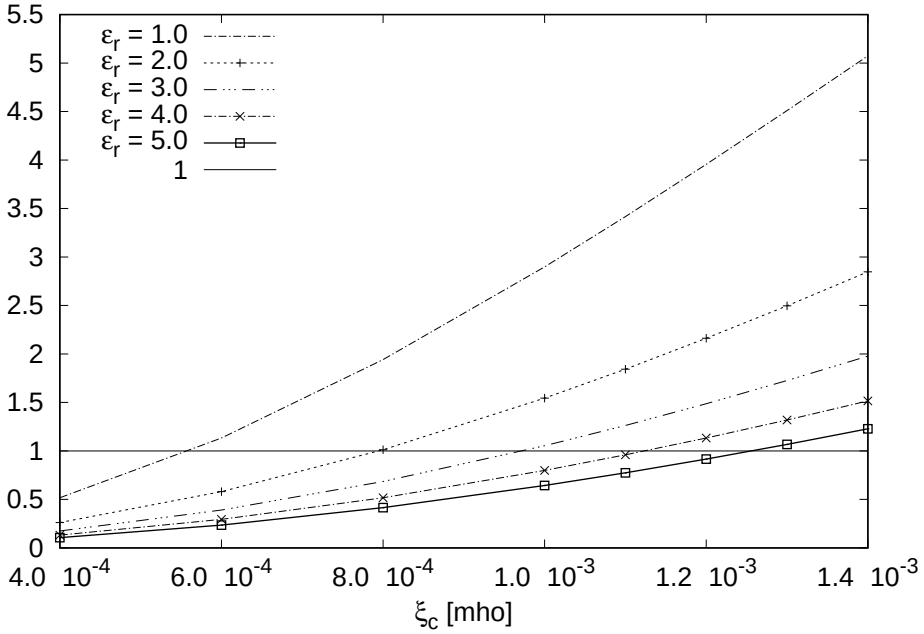


Figure 8: Plot of $K_u$ versus $\xi_c$ for the bianisotropic medium described in [5]. The plots are shown for various values of $\varepsilon_r$. The hypothesis H4 is satisfied for $K_u < 1$.

$$C_{\kappa,r} = \varepsilon_0 \varepsilon_r \tag{64}$$

$$C_{\nu,r} = \frac{\mu_0 \varepsilon_0 \varepsilon_r}{\varepsilon_0 \varepsilon_r + \mu_0 \xi_c^2} \tag{65}$$

From equations (28) and (29) we get

$$C_{\chi,s} = C_{\gamma,s} = \frac{\xi_c}{\varepsilon_0 \varepsilon_r}. \tag{66}$$

Having shown that the hypotheses H1-H3 are satisfied, we can use the above constants to calculate $K_u$ and then to verify H4. Figure 8 shows the dependence of $K_u$ on $\xi_c$ for various values of $\varepsilon_r$. As the value of $\varepsilon_r$ increases, the hypothesis H4 remains valid for higher and higher value of $\xi_c$. Figure 9 shows the plot of the critical value of $\xi_c$ below which H4 is satisfied against $\varepsilon_r$. The limit of $2.654\,10^{-3}$ arising from equation (56) required for satisfying H7 is also shown in the same figure. It is seen that for low values of $\varepsilon_r$ the tighter condition arises from the need to satisfy H4. For example the limiting value is $5.6\,10^{-4}$ for $\varepsilon_r = 1$ and increases with $\varepsilon_r$ and is $1.78\,10^{-3}$ for $\varepsilon_r = 10$. The curve crosses $2.654\,10^{-3}$ mho line at around $\varepsilon_r = 22.3$ and above that value equation (56) imposes the stricter limit.

Now we consider a specific numerical problem for which the solution can serve as benchmark for other approaches and solvers owing to the reliability of the results guaranteed by the theory. A rectangular waveguide with a discontinuity due to a block of bianisotropic medium is considered as shown in Figure 10. In the simulation the rectangular waveguide is characterized by $a = 23$ mm, $b = 10$ mm and has a length $l = 40$ mm. The obstacle is a parallelepiped with $c = 11$ mm,

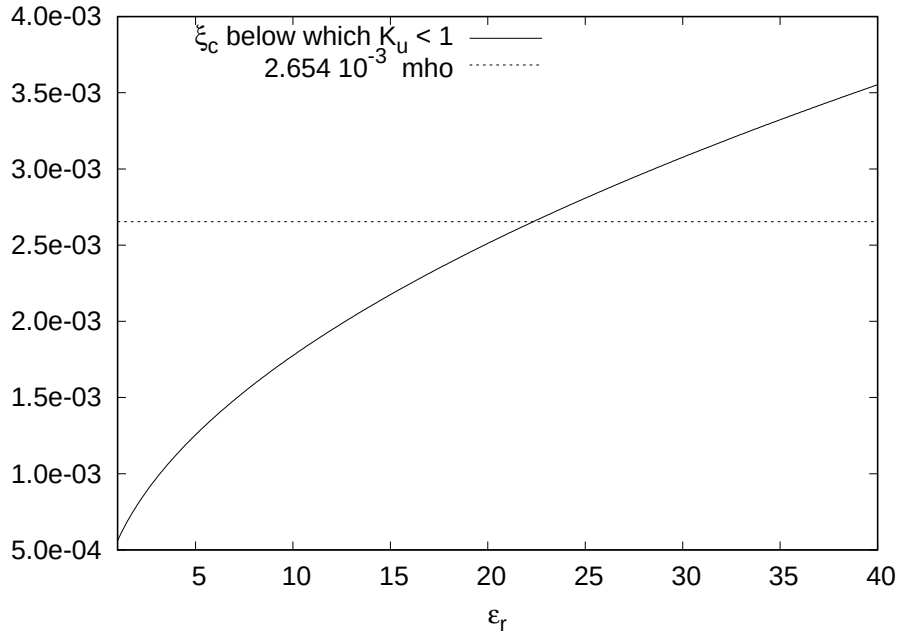


Figure 9: The value of $\xi_c$ below which the hypothesis H4 is satisfied is plotted against $\varepsilon_r$. The limit of $2.654\,10^{-3}$ arising from equation (56) required for satisfying H7 is also shown.

$d = 5$ mm and length $w = 10$ mm. The origin of the axis is at the lower right corner of the near face of the waveguide shown in Figure 10. The obstacle ranges from $x = 6$ mm to $x = 17$ mm along the x axis, from $y = 0$ to $y = 5$ mm along the y axis and from $z = 15$ mm to $z = 25$ mm along the z axis. The bianisotropic medium making up the obstacle is characterized by $\varepsilon_r = 5$ and $\xi_c = 1.24\,10^{-3}$. For this medium $K_u = 0.98 < 1$ and also equation (56) is satisfied and hence all the hypotheses required to guarantee the well posedness and convergence of finite element solution hold true. The waveguide is excited with $TE_{10}$ mode with amplitude of 1 $V/m$ and frequency of 9 GHz.

The details of the Galerkin finite element solver is the same as before. The tetrahedral meshes are also obtained in a similar way as discussed in the previous subsection by dividing the domain into small cubes each of which are in turn subdivided into six tetrahedra. The convergence of the solution is verified by checking the solutions for three different meshes which are characterized by small cubes of sides 0.5 mm, 0.25 mm and 0.167 mm which are references as, respectively, "coarse", "fine" and "very fine" meshes. There are 10824 nodes, 55200 elements and 6200 boundary faces in coarse mesh, where as the fine mesh has 79947 nodes, 441600 elements and 24800 boundary faces and finally the very fine mesh has 262570 nodes, 1490400 elements and 55800 boundary faces. The solutions obtained were very stable which is illustrated by showing the results obtained for the x component of the magnitude of the electric field along the y axis with these meshes in Figure 11.

Figures 12 to 14 show the results for the magnitudes and phases of the components of the electric field along the x axis. The effect on the fields due to bianisotropic effects are not negligible for both the magnitude and phase. We have, for example, a difference of 20 percent of the magnitude of incident field for the x component of the electric field along the x axis.

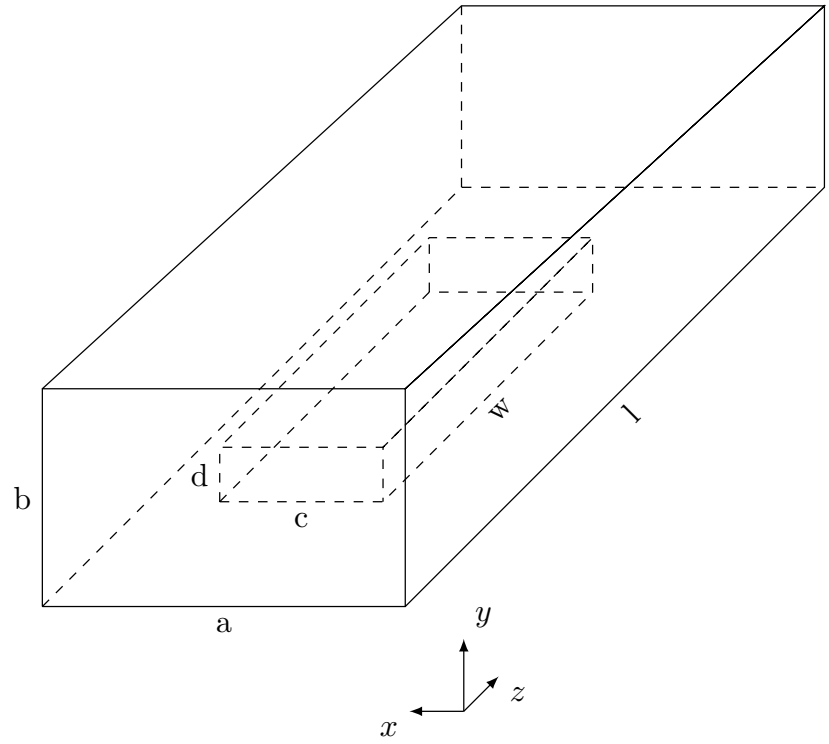


Figure 10: The geometry of a rectangular waveguide partially filled with chiral media considered in [5].

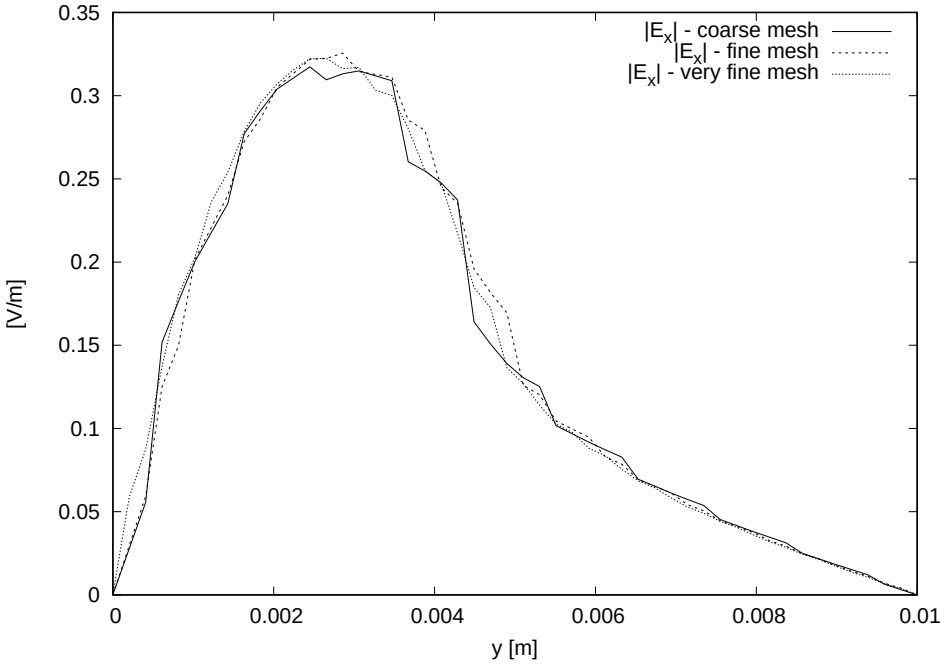


Figure 11: Convergence of the solution for problem involving medium in [5]. The magnitude of the $x$ component of the electric field is plotted along a line parallel to $y$ axis for four different meshes.

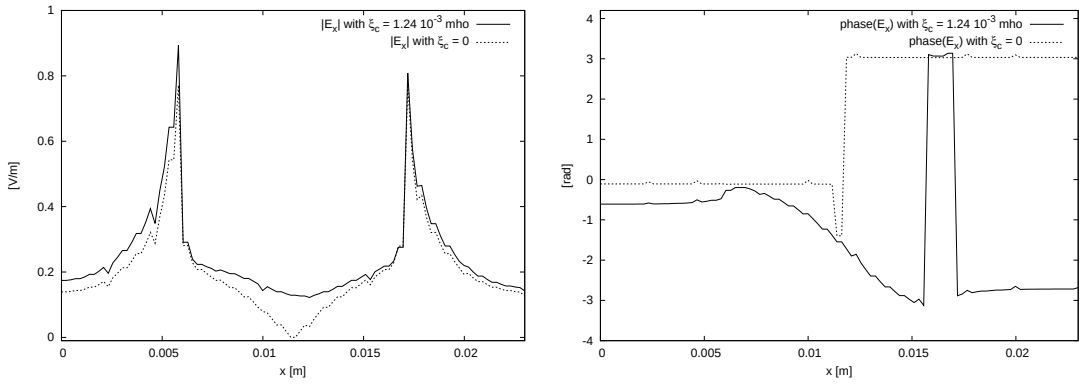


Figure 12: The magnitude and phase of the $x$ component of electric field along a line parallel to $x$ axis and passing though the center of gravity of the domain for problem involving medium in [5]. The plot for bianisotropic case using $\xi_c = 1.24\,10^{-3}$ mho is compared with the solution obtained in isotropic case using $\xi_c = 0$.

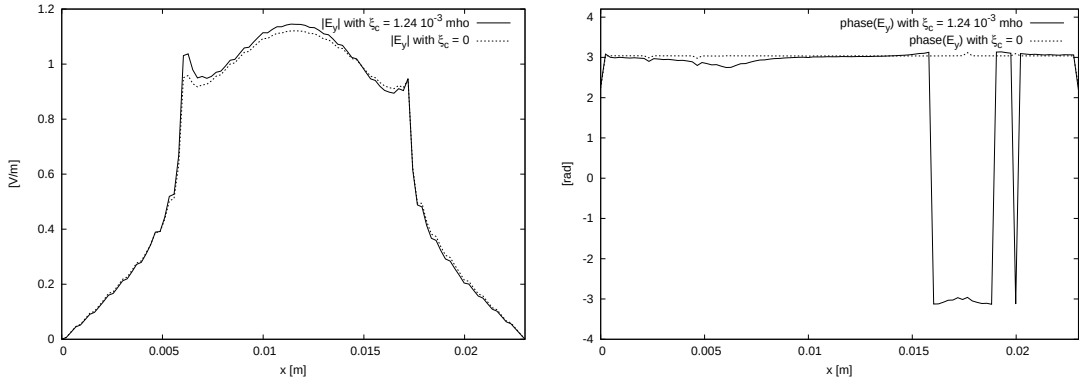


Figure 13: The magnitude and phase of the $y$ component of electric field along a line parallel to $x$ axis and passing though the center of gravity of the domain for problem involving medium in [5]. The plot for bianisotropic case using $\xi_c = 1.24\,10^{-3}$ mho is compared with the solution obtained in isotropic case using $\xi_c = 0$.

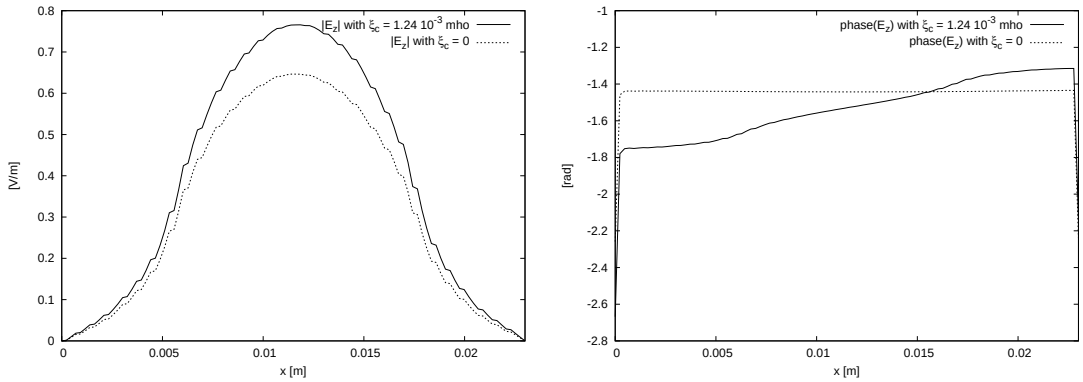


Figure 14: The magnitude and phase of the $z$ component of electric field along a line parallel to $x$ axis and passing though the center of gravity of the domain for problem involving medium in [5]. The plot for bianisotropic case using $\xi_c = 1.24\,10^{-3}$ mho is compared with the solution obtained in isotropic case using $\xi_c = 0$.

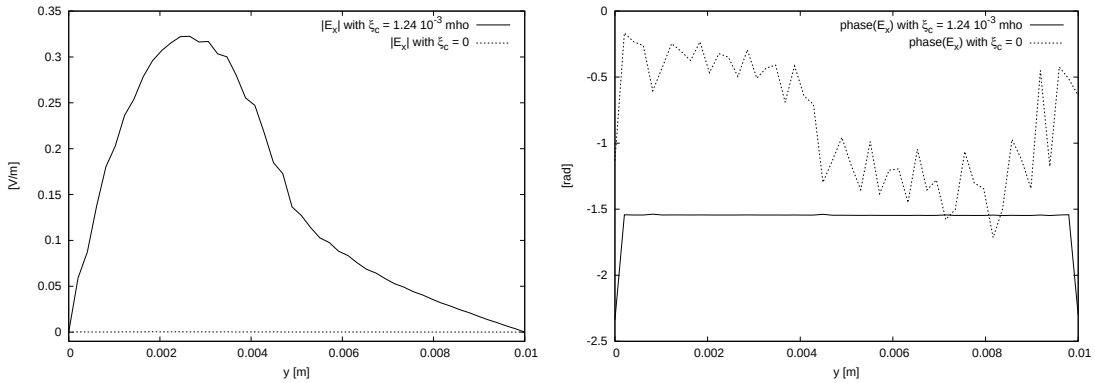


Figure 15: The magnitude and phase of the $x$ component of electric field along a line parallel to $y$ axis and passing though the center of gravity of the domain for problem involving medium in [5]. The plot for bianisotropic case using $\xi_c = 1.24\,10^{-3}$ mho is compared with the solution obtained in isotropic case using $\xi_c = 0$.

Similar results are shown in Figures 15 to 20 for the components of fields along y and z directions. The bianisotropic effect cause a difference of more than 30 percent of the incident field as can be seen from Figure 15.

As mentioned earlier, together, these results provide a bench mark for other approaches to solving such problems, owing to the reliability of the results provided here which is guaranteed by the recently developed theory. The previous theory [3] was not able to manage these problems and our results are therefore novel. The significant bianisotropic effects demonstrated in the results show the practical importance of the theory for such media.

### 3.3 Bianisotropic media considered in [6]

Another instance of a relevant bianisotropic media was considered in [6], where the authors consider a rectangular waveguide, half of which is empty and the other half is filled with a lossless bianisotropic material characterized by

$$P = \varepsilon_0 c_0 I_3, \tag{67}$$

$$Q = \frac{1}{\mu_0 c_0} I_3, \tag{68}$$

$$L = M = j\kappa_0 A, \tag{69}$$

where $A$ is the matrix given by

$$A = \begin{bmatrix} 1 & 1 & 0 \\ 1 & 1 & 0 \\ 0 & 0 & 1 \end{bmatrix}, \tag{70}$$

where $\kappa_0$ is a positive real number.

The hypotheses H5 and H6 are trivially valid with $C_{PS} = \varepsilon_0 c_0$ and $C_{QS} = \frac{1}{\mu_0 c_0}$. Further, $L^*L = M^*M = \kappa_0^2 A^2$ whose eigenvalues are 0, $\kappa_0^2$ and $4\kappa_0^2$. Therefore by equations (18) and

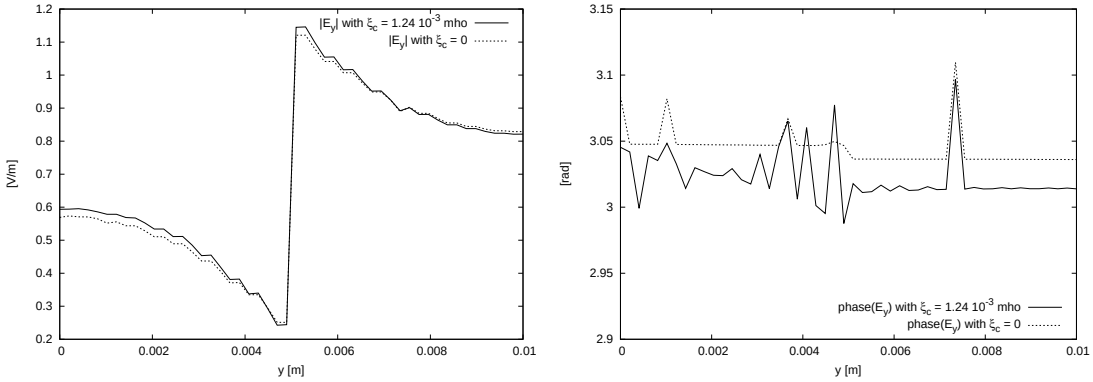


Figure 16: The magnitude and phase of the $y$ component of electric field along a line parallel to $y$ axis and passing though the center of gravity of the domain for problem involving medium in [5]. The plot for bianisotropic case using $\xi_c = 1.24\,10^{-3}$ mho is compared with the solution obtained in isotropic case using $\xi_c = 0$.

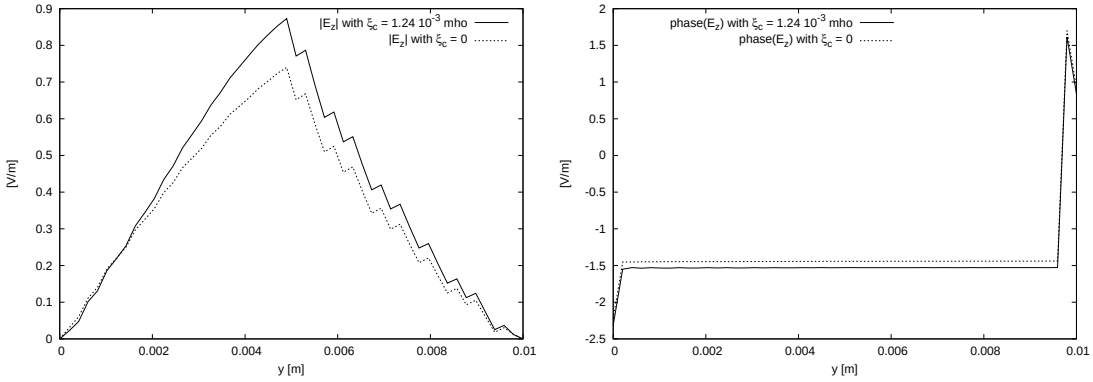


Figure 17: The magnitude and phase of the $z$ component of electric field along a line parallel to $y$ axis and passing though the center of gravity of the domain for problem involving medium in [5]. The plot for bianisotropic case using $\xi_c = 1.24\,10^{-3}$ mho is compared with the solution obtained in isotropic case using $\xi_c = 0$.

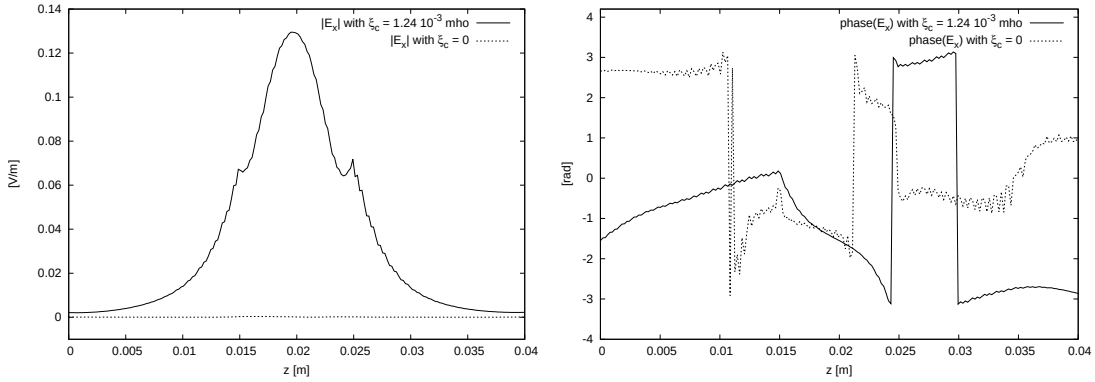


Figure 18: The magnitude and phase of the $x$ component of electric field along a line parallel to $z$ axis and passing though the center of gravity of the domain for problem involving medium in [5]. The plot for bianisotropic case using $\xi_c = 1.24\,10^{-3}$ mho is compared with the solution obtained in isotropic case using $\xi_c = 0$.

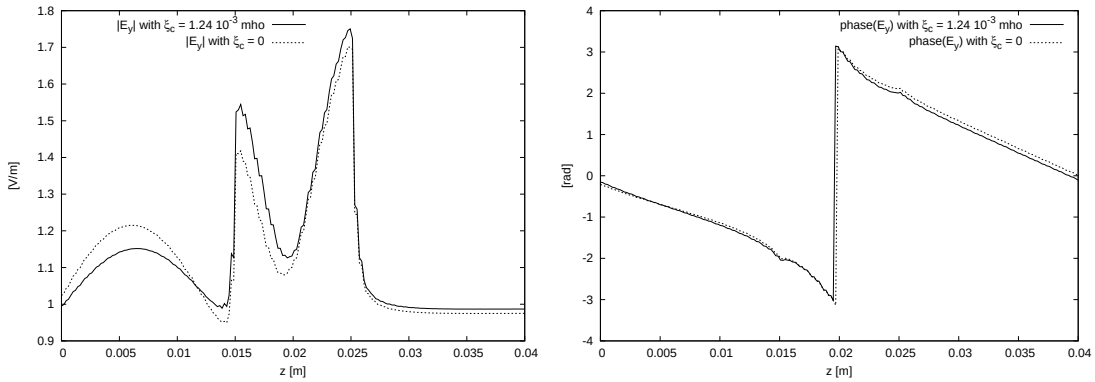


Figure 19: The magnitude and phase of the $y$ component of electric field along a line parallel to $z$ axis and passing though the center of gravity of the domain for problem involving medium in [5]. The plot for bianisotropic case using $\xi_c = 1.24\,10^{-3}$ mho is compared with the solution obtained in isotropic case using $\xi_c = 0$.

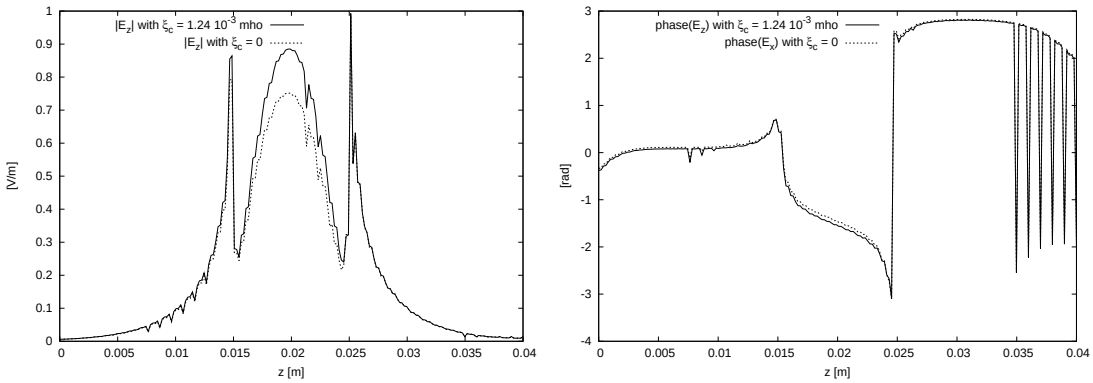


Figure 20: The magnitude and phase of the $z$ component of electric field along a line parallel to $z$ axis and passing though the center of gravity of the domain for problem involving medium in [5]. The plot for bianisotropic case using $\xi_c = 1.24\,10^{-3}$ mho is compared with the solution obtained in isotropic case using $\xi_c = 0$.

(19) we get $C_L = C_M = 2\kappa_0$. The condition in hypothesis H7 then becomes $C_{QS} - \frac{C_L C_M}{C_{PS}} = \frac{1}{\mu_0 c_0} - \frac{4\kappa_0^2}{\varepsilon_0 c_0} > 0$, which gives the following limit on $\kappa_0$.

$$\kappa_0 < \frac{1}{2}\sqrt{\frac{\varepsilon_0}{\mu_0}} = 1.327\,10^{-3} \text{ mho} \tag{71}$$

The hypotheses H1 to H4 can be studied using the alternative form of constitutive relations which is characterized by the following matrices [7].

$$\kappa = \frac{1}{\varepsilon_0} I_3 \tag{72}$$

$$\nu = \frac{1}{\mu_0} I_3 + \frac{\kappa_0^2}{\varepsilon_0} A^2 \tag{73}$$

$$\chi = -\gamma = \frac{-j\kappa_0}{\varepsilon_0} A \tag{74}$$

The determinants of $\kappa$ and $\nu$ can be readily calculated and by using equations (20) and (21) we get $C_{\kappa,d}$ and $C_{\nu,d}$.

$$C_{\kappa,d} = \frac{1}{\varepsilon_0^3} \tag{75}$$

$$C_{\nu,d} = \frac{(\varepsilon_0 + \mu_0\kappa_0^2)(\varepsilon_0 + 4\mu_0\kappa_0^2)}{\mu_0^3 \varepsilon_0^2} \tag{76}$$

$C_{\kappa,s}$ and $C_{\nu,s}$ can be directly obtained from their definitions.

$$C_{\kappa,s} = \frac{2}{\varepsilon_0} \tag{77}$$

$$C_{\nu,s} = \frac{2\varepsilon_0 + 8\mu_0\kappa_0^2}{\mu_0\varepsilon_0} \tag{78}$$

By simple application of the definition

$$C_{\kappa,r} = \varepsilon_0, \tag{79}$$

and by equation (27) $C_{\nu,r}$ evaluates to the reciprocal of the largest eigenvalue of the real matrix $\nu$ which is given by

$$C_{\nu,r} = \frac{\mu_0\varepsilon_0}{\varepsilon_0 + 4\mu_0\kappa_0^2}. \tag{80}$$

The equations (28) and (29) give

$$C_{\chi,s} = C_{\gamma,s} == \frac{4\kappa_0}{\varepsilon_0}. \tag{81}$$

The existence of the above constants verifies H1 -H3 and we can use them to calculate $K_u$ to verify H4. It can be verified that $K_u$ is less than one when $\kappa_0 \leq 2.72\,10^{-4}$ mho, which is stricter than the limit obtained from equation (71).

Finally let us give some numerical solutions for this problem, which can be used as benchmarks for other approaches. The cross section of the waveguide is such that it is 2 cm along the x axis and 1 cm along the y axis, and the length of the waveguide is 2 cm, half of which is filled with the bianisotropic medium characterized by $\kappa_0 = 2.7\,10^{-3}$. The origin is taken on the corner of the open face of the waveguide on the empty side. $TE_{10}$ mode is excited in the waveguide with source of amplitude 1 $V/m$ and frequency of 12 GHz.

First order edge element based Galerkin finite element method is used to obtain the solution. The meshing is carried out by dividing the domain into identical cubes each of which are then subdivided into six tetrahedra. Convergence is ensured by evaluating the solutions on three meshes, termed as "coarse", "fine" and "very fine" characterized, respectively, by cubes of sides 1 mm, 0.5 mm and 0.33 mm. The coarse mesh had 4852 nodes, 24000 elements and 3200 boundary faces. The fine mesh is composed of 35301 nodes, 192000 elements and 12800 boundary faces. The very fine mesh has 115351 nodes, 648000 elements and 28800 boundary faces. Figure 21 shows the results obtained on the three meshes for the x component of the electric field along the y axis and confirms the stability of the solutions.

We provide the magnitudes and phases of the components of the electric field obtained from the simulation in Figures 22 to 30. It can be observed that the bianisotropic effects are non negligible and the largest effects are on the x component of the field. The bianisotropy causes a difference in magnitude of up to 14 percent of the incident field, as can be seen, for example, from Figure 22, 25 or 28. Since the theory guarantees the reliability of these results, it can be used as benchmark for other solvers and approaches.

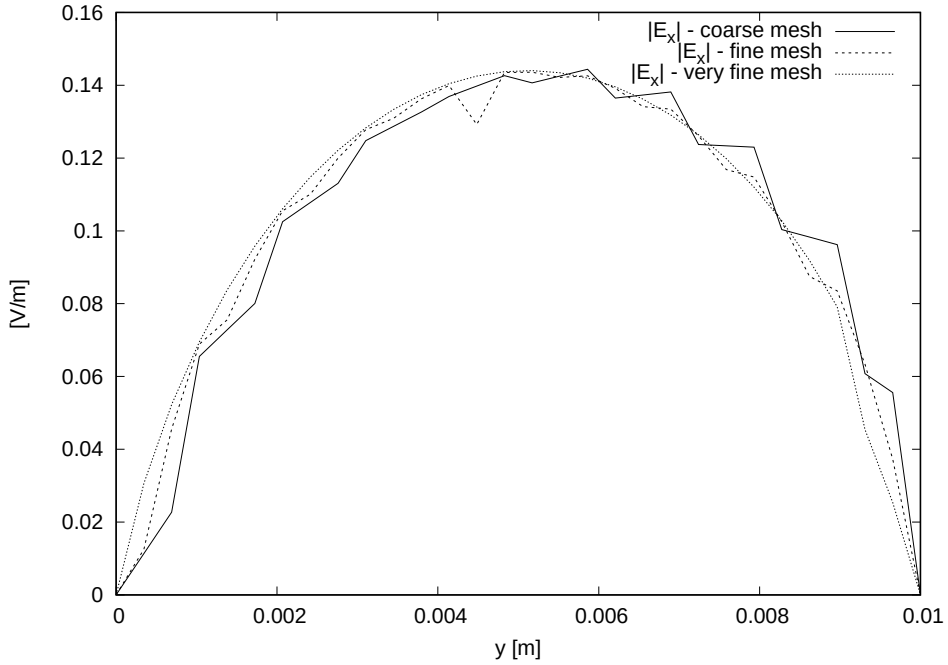


Figure 21: Convergence of the solution for problem involving medium in [6]. The magnitude of the $x$ component of the electric field is plotted along a line parallel to $y$ axis for four different meshes.

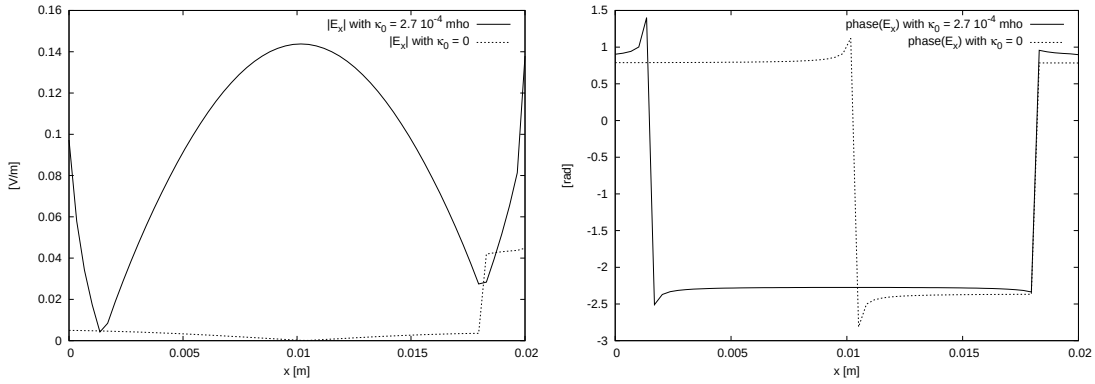


Figure 22: The magnitude and phase of the $x$ component of electric field along a line parallel to $x$ axis and passing though the center of gravity of the domain for problem involving medium in [6]. The plot for bianisotropic case using $\kappa_0 = 2.7\,10^{-4}$ mho is compared with the solution obtained in isotropic case using $\kappa_0 = 0$.

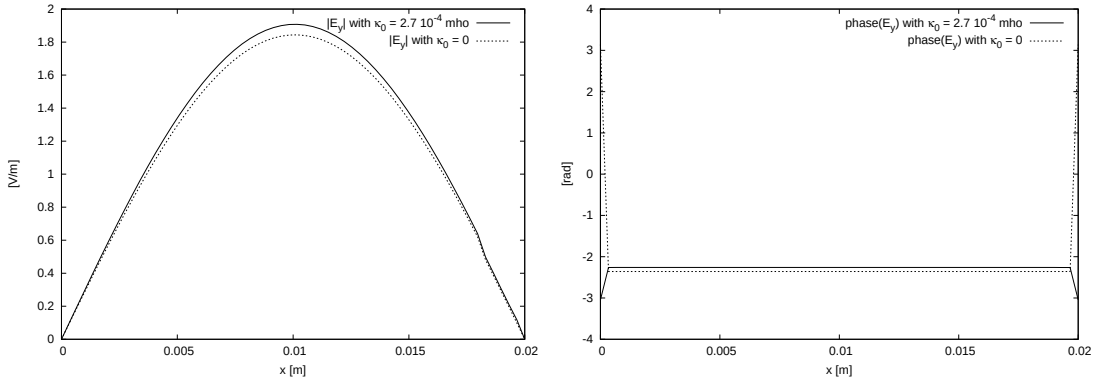


Figure 23: The magnitude and phase of the $y$ component of electric field along a line parallel to $x$ axis and passing though the center of gravity of the domain for problem involving medium in [6]. The plot for bianisotropic case using $\kappa_0 = 2.7\,10^{-4}$ mho is compared with the solution obtained in isotropic case using $\kappa_0 = 0$.

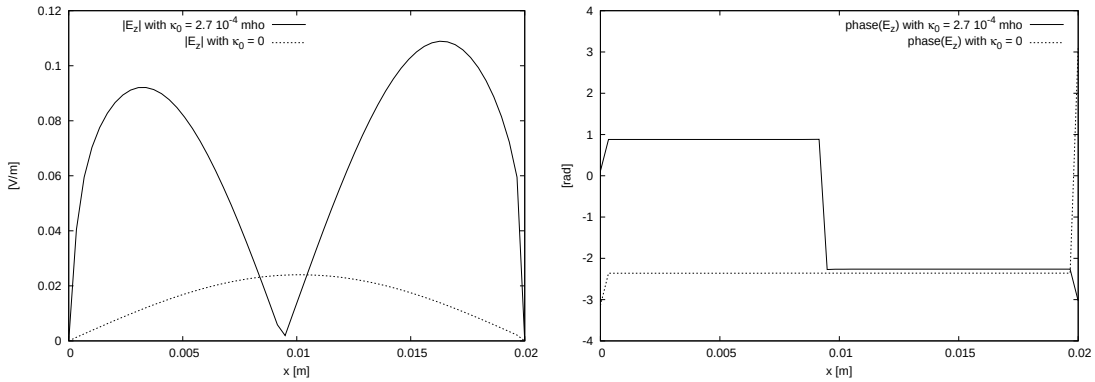


Figure 24: The magnitude and phase of the $z$ component of electric field along a line parallel to $x$ axis and passing though the center of gravity of the domain for problem involving medium in [6]. The plot for bianisotropic case using $\kappa_0 = 2.7\,10^{-4}$ mho is compared with the solution obtained in isotropic case using $\kappa_0 = 0$.

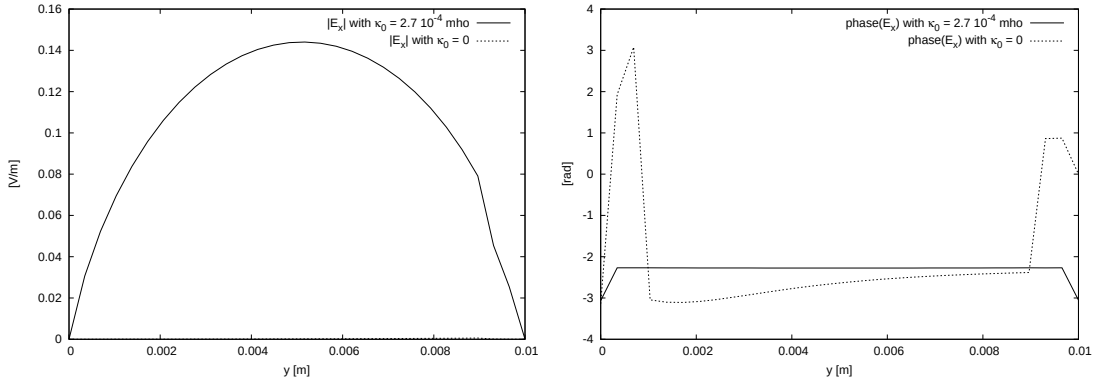


Figure 25: The magnitude and phase of the $x$ component of electric field along a line parallel to $y$ axis and passing though the center of gravity of the domain for problem involving medium in [6]. The plot for bianisotropic case using $\kappa_0 = 2.7\,10^{-4}$ mho is compared with the solution obtained in isotropic case using $\kappa_0 = 0$.

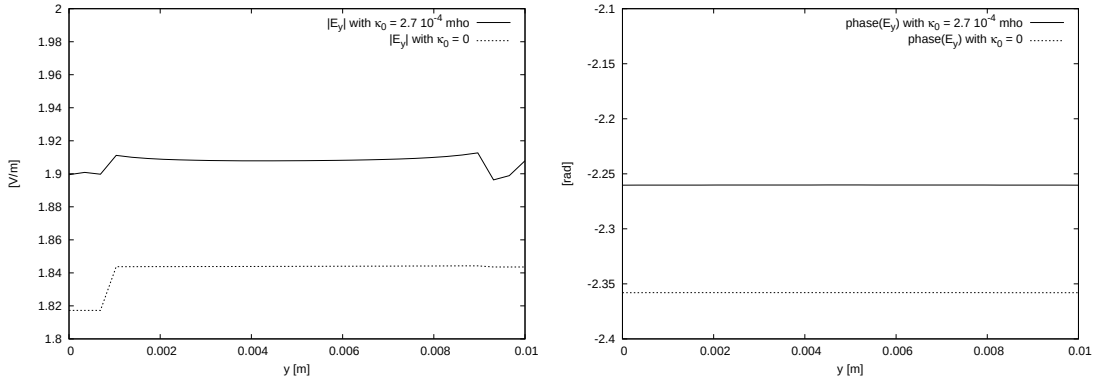


Figure 26: The magnitude and phase of the $y$ component of electric field along a line parallel to $y$ axis and passing though the center of gravity of the domain for problem involving medium in [6]. The plot for bianisotropic case using $\kappa_0 = 2.7\,10^{-4}$ mho is compared with the solution obtained in isotropic case using $\kappa_0 = 0$.

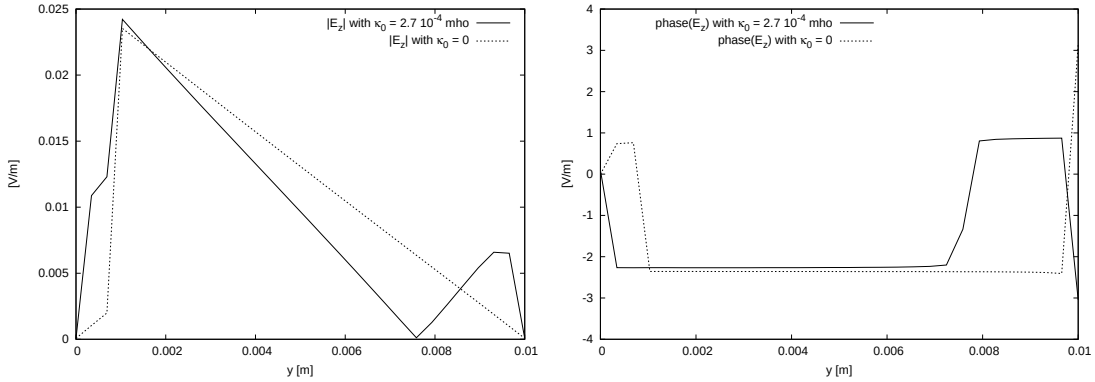


Figure 27: The magnitude and phase of the $z$ component of electric field along a line parallel to $y$ axis and passing though the center of gravity of the domain for problem involving medium in [6]. The plot for bianisotropic case using $\kappa_0 = 2.7\,10^{-4}$ mho is compared with the solution obtained in isotropic case using $\kappa_0 = 0$.

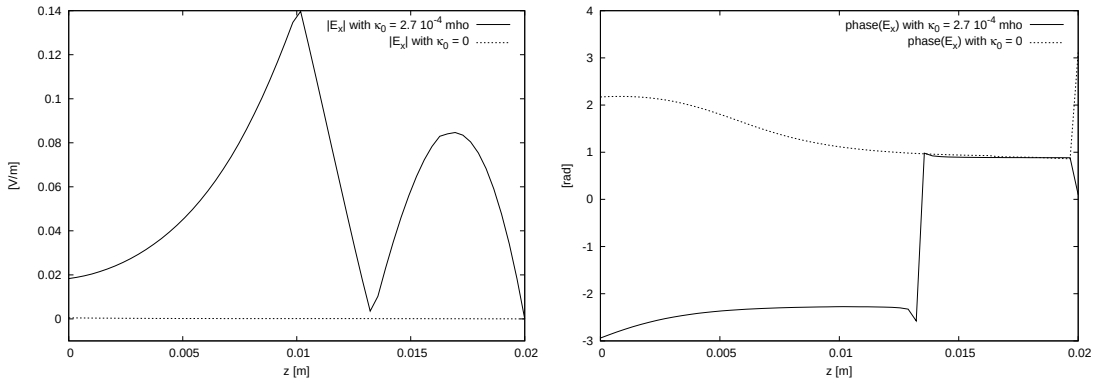


Figure 28: The magnitude and phase of the $x$ component of electric field along a line parallel to $z$ axis and passing though the center of gravity of the domain for problem involving medium in [6]. The plot for bianisotropic case using $\kappa_0 = 2.7\,10^{-4}$ mho is compared with the solution obtained in isotropic case using $\kappa_0 = 0$.

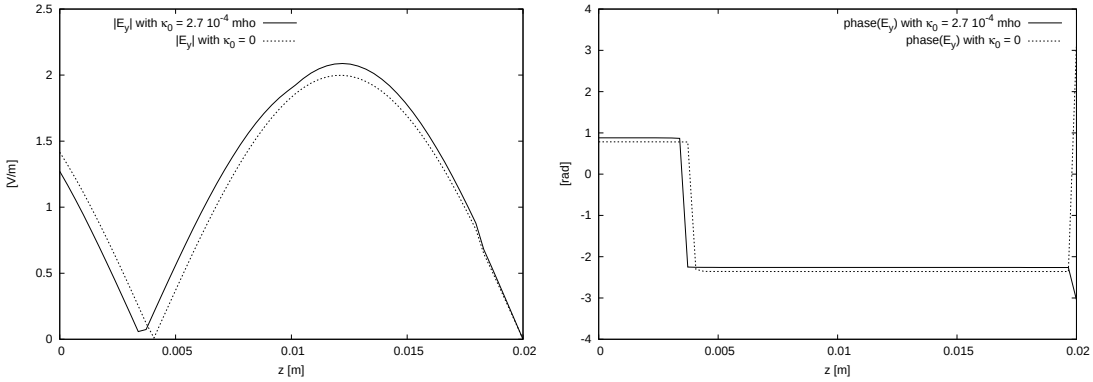


Figure 29: The magnitude and phase of the $y$ component of electric field along a line parallel to $z$ axis and passing though the center of gravity of the domain for problem involving medium in [6]. The plot for bianisotropic case using $\kappa_0 = 2.7\,10^{-4}$ mho is compared with the solution obtained in isotropic case using $\kappa_0 = 0$.

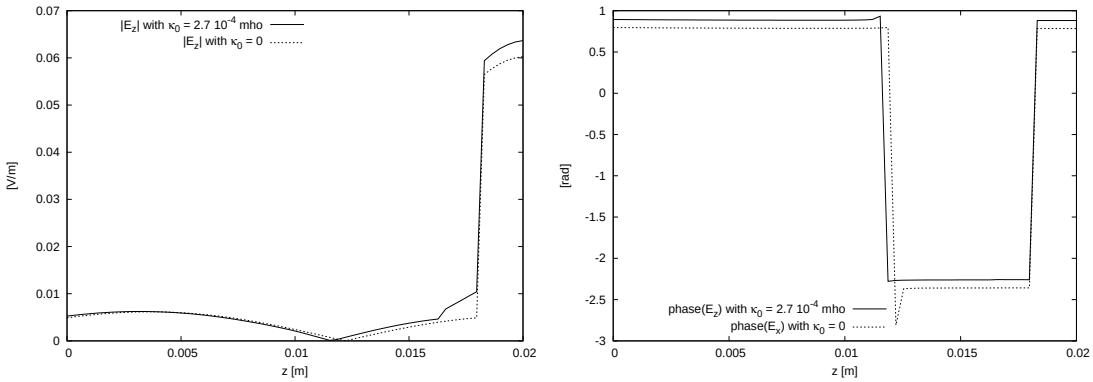


Figure 30: The magnitude and phase of the $z$ component of electric field along a line parallel to $z$ axis and passing though the center of gravity of the domain for problem involving medium in [6]. The plot for bianisotropic case using $\kappa_0 = 2.7\,10^{-4}$ mho is compared with the solution obtained in isotropic case using $\kappa_0 = 0$.

# 4 Conclusions

# References


[1] P. Kalarickel Ramakrishnan and M. Raffetto, "Well posedness and finite element approximability of three-dimensional time-harmonic electromagnetic problems involving rotating axisymmetric objects," *Symmetry*, vol. 12, no. 2, p. 218, 2020.

[2] P. Monk, *Finite element methods for Maxwell's equations*. Oxford: Oxford Science Publications, 2003.

[3] P. Fernandes and M. Raffetto, "Well posedness and finite element approximability of time-harmonic electromagnetic boundary value problems involving bianisotropic materials and metamaterials," *Mathematical Models and Methods in Applied Sciences*, vol. 19, no. 12, pp. 2299–2335, December 2009, DOI No: 10.1142/S0218202509004121.

[4] M. Kraft, A. Braun, Y. Luo, S. A. Maier, and J. B. Pendry, "Bianisotropy and magnetism in plasmonic gratings," *ACS Photonics*, vol. 3, no. 5, pp. 764–769, 2016.

[5] T. X. Wu and D. L. Jaggard, "A comprehensive study of discontinuities in chirowaveguides," *IEEE Transactions on Microwave Theory and Techniques*, vol. 50, no. 10, pp. 2320–2330, October 2002.

[6] P. Alotto and L. Codecasa, "A fit formulation of bianisotropic materials over polyhedral grids," *IEEE Transactions on Magnetics*, vol. 50, no. 2, pp. 349–352, February 2014.

[7] P. Fernandes, M. Ottonello, and M. Raffetto, "Regularity of time-harmonic electromagnetic fields in the interior of bianisotropic materials and metamaterials," *The IMA Journal of Applied Mathematics*, vol. 79, no. 1, pp. 54–93, February 2014.

[8] X. Chen, B.-I. Wu, J. A. Kong, and T. M. Grzegorczyk, "Retrieval of the effective constitutive parameters of bianisotropic metamaterials," *Physical Review E*, vol. 71, no. 4, p. 046610, 2005.

[9] Z. Li, K. Aydin, and E. Ozbay, "Determination of the effective constitutive parameters of bianisotropic metamaterials from reflection and transmission coefficients," *Physical review E*, vol. 79, no. 2, p. 026610, 2009.

[10] P. G. Ciarlet and J. L. L. (Eds.), *Handbook of Numerical Analysis, vol. II, Finite Element Methods, Part 1*. Amsterdam: North-Holland, 1991.